

Doping-Induced Ferromagnetism and Possible Triplet Pairing in d^4 Mott Insulators

Jiří Chaloupka¹ and Giniyat Khaliullin²

¹*Central European Institute of Technology, Masaryk University, Kotlářská 2, 61137 Brno, Czech Republic*

²*Max Planck Institute for Solid State Research, Heisenbergstrasse 1, D-70569 Stuttgart, Germany*

(Dated: September 17, 2018)

We study the effects of electron doping in Mott insulators containing d^4 ions such as Ru^{4+} , Os^{4+} , Rh^{5+} , and Ir^{5+} with $J = 0$ singlet ground state. Depending on the strength of the spin-orbit coupling, the undoped systems are either nonmagnetic or host an unusual, excitonic magnetism arising from a condensation of the excited $J = 1$ triplet states of t_{2g}^4 . We find that the interaction between J -excitons and doped carriers strongly supports ferromagnetism, converting both the nonmagnetic and antiferromagnetic phases of the parent insulator into a ferromagnetic metal, and further to a nonmagnetic metal. Close to the ferromagnetic phase, the low-energy spin response is dominated by intense paramagnon excitations that may act as mediators of a triplet pairing.

PACS numbers: 75.10.Jm, 75.25.Dk, 75.30.Et, 74.10.+v

A distinct feature of Mott insulators is the presence of low-energy magnetic degrees of freedom, and their coupling to doped charge carriers plays the central role in transition metal compounds [1]. In large spin systems like manganites, this coupling converts parent antiferromagnet (AF) into a ferromagnetic (FM) metal and gives rise to large magnetoresistivity effects. The doping of spin one-half compounds like cuprates and titanites, on the other hand, suppresses magnetic order and a paramagnetic (PM) metal emerges. In general, the fate of magnetism upon charge doping is dictated by spin-orbital structure of parent insulators.

In compounds with an even number of electrons on the d shell, one may encounter a curious situation when the ionic ground state has no magnetic moment at all, yet they may order magnetically by virtue of low-lying magnetic levels with finite spin, if the exchange interactions are strong enough to overcome single-ion magnetic gap. The d^4 ions such as Ru^{4+} , Os^{4+} , Rh^{5+} , Ir^{5+} possess exactly this type level structure [2] due to spin-orbit coupling $\lambda(\mathbf{S} \cdot \mathbf{L})$: the spin $S = 1$ and orbital $L = 1$ moments form a nonmagnetic ground state with total $J = 0$ moment, separated from the excited level $J = 1$ by λ . A competition of the exchange and spin-orbit couplings results then in a quantum critical point (QCP) between nonmagnetic Mott insulator and magnetic order [3, 4]. Since magnetic order is due to condensation of the virtual $J = 1$ levels and hence “soft”, the amplitude (Higgs) mode is expected. The corollary of the “ d^4 excitonic magnetism” [3] is the presence of magnetic QCP that does not require any special lattice geometry, and the energy scales involved are large. The recent neutron scattering data [5] in d^4 Ca_2RuO_4 seem to support the theoretical expectations.

As we show in this Letter, unusual magnetism of d^4 insulators, where the “soft” J -spins fluctuate between 0 and 1, results also in anomalous doping effects that differ drastically from conventional cases as manganites and cuprates. Indeed, while common wisdom suggests

that the PM phase with yet uncondensed J -moments near QCP would get even “more PM” upon doping, we find that mobile carriers induce long-range order instead. The order is of FM type and is promoted by carrier-driven condensation of J -moments. By the same mechanism, the exchange dominated AF phase also readily switches to FM metal, as observed in La-doped Ca_2RuO_4 [6, 7]. The theory might be relevant also to electric-field-induced FM of Ca_2RuO_4 [8] and FM state of the RuO_2 planes in oxide superlattices [9]. Further doping suppresses any magnetic order, and we suggest that residual FM correlations may lead to a triplet superconductivity (SC).

Model.— There are a number of d^4 compounds, magnetic as well nonmagnetic, with various lattice structures [10–17]. To be specific, we consider a square lattice d^4 insulator lightly doped by electrons. Assuming relatively large spin-orbit coupling (SOC), the relevant states are pseudospin $J = 0, 1$ states of t_{2g}^4 and $J = 1/2$ states of t_{2g}^5 [see Fig. 1(a)]. The d^4 singlet s ($J = 0$) and triplon $T_{0,\pm 1}$ ($J = 1$) states obey the Hamiltonian derived in Ref. 3. Adopting the Cartesian basis $T_x = (T_1 - T_{-1})/\sqrt{2}i$, $T_y = (T_1 + T_{-1})/\sqrt{2}$, and $T_z = iT_0$, it can be written as

$$\mathcal{H}_{d^4} = \lambda \sum_i \mathbf{T}_i^\dagger \cdot \mathbf{T}_i + \frac{1}{4}K \sum_{\langle ij \rangle} \left[s_i s_j^\dagger (\mathbf{T}_i^\dagger \cdot \mathbf{T}_j - \frac{1}{3}T_{i\gamma}^\dagger T_{j\gamma}) - s_i^\dagger s_j (\frac{5}{6}\mathbf{T}_i \cdot \mathbf{T}_j - \frac{1}{6}T_{i\gamma} T_{j\gamma}) + \text{H.c.} \right], \quad (1)$$

where γ is determined by the bond direction. The model shows AF transition due to a condensation of \mathbf{T} at a critical value $K_c = \frac{6}{11}\lambda$ of the interaction parameter $K = 4t_0^2/U$. The degenerate $T_{x,y,z}$ levels split upon material-dependent lattice distortion, affecting the details of the model behavior [19]. We will consider the cubic symmetry case and make a few comments on the possible effects of the tetragonal splitting.

The d^4 system is doped by introducing a small amount of d^5 objects – fermions f_σ carrying the pseudospin $J = 1/2$ of t_{2g}^5 . The on-site constraint $n_s + n_T + n_f = 1$ is

implied. The Hamiltonian describing the correlated motion of f is derived by calculating matrix elements of the nearest-neighbor hopping $\hat{T}_{ij} = -t_0(a_{i\sigma}^\dagger a_{j\sigma} + b_{i\sigma}^\dagger b_{j\sigma})$ between multielectron configurations $\langle d_i^5 d_j^4 | \hat{T}_{ij} | d_i^4 d_j^5 \rangle$. Here a and b are the t_{2g} orbitals active on a given bond, *e.g.* xy and zx for x -bonds. The resulting hopping Hamiltonian comprises three contributions, $\mathcal{H}_{d^4-d^5} = \sum_{ij} (h_1 + h_2 + h_3)_{ij}^{(\gamma)}$. The first one, depicted schematically in Fig. 1(b,c), is a spin-independent motion of f , accompanied by a backflow of s and T :

$$h_1^{(\gamma)} = -t f_{i\sigma}^\dagger f_{j\sigma} \left[s_j^\dagger s_i + \frac{15}{16} (\mathbf{T}_j^\dagger \cdot \mathbf{T}_i - \frac{3}{5} T_{j\gamma}^\dagger T_{i\gamma}) \right]. \quad (2)$$

The second contribution is a spin-dependent motion of f generating $J=0 \leftrightarrow J=1$ magnetic excitation in the d^4 background [see Fig. 1(d)]:

$$h_2^{(\gamma)} = i\tilde{t} \left[\sigma_{ij}^\gamma (s_j^\dagger T_{i\gamma} - T_{j\gamma}^\dagger s_i) - \frac{1}{3} \sigma_{ij} \cdot (s_j^\dagger \mathbf{T}_i - \mathbf{T}_j^\dagger s_i) \right]. \quad (3)$$

Here, $\sigma_{ij} = f_{i\alpha}^\dagger \tau_{\alpha\beta} f_{j\beta}$ with Pauli matrices τ denotes the bond-spin operator. The derivation for the cubic symmetry gives $t = \frac{4}{9}t_0$ and $\tilde{t} = \frac{1}{\sqrt{6}}t_0$ with the ratio $\tilde{t}/t \approx 1$. However, these values are affected by the lattice distortions (via the pseudospin wave functions) and f -band renormalization reducing the effective t . We thus consider \tilde{t}/t as a free parameter and set $\tilde{t} = 1.5t$ below. The last contribution to $\mathcal{H}_{d^4-d^5}$ reads as coupling between the bond-spins residing in f and T sectors: $h_3^{(\gamma)} = \frac{9}{16}t (\sigma_{ij}^\gamma J_{ji}^\gamma + \frac{1}{3} \sigma_{ij} \cdot \mathbf{J}_{ji})$, where $\mathbf{J}_{ji} = -i(\mathbf{T}_j^\dagger \times \mathbf{T}_i)$. At small doping and near QCP where the density of T excitons is small, the scattering term h_3 can be neglected.

Phase diagram.— We first inspect the phase behavior of the model as a function of doping x and interaction parameters K and \tilde{t} . The magnetic order is linked to the condensation of triplons induced by their mutual interactions and the interaction with the doped fermions f . In contrast to the cubic lattice where all the T flavors are equivalent, on the two-dimensional square lattice the T_z flavor experiences the strongest interactions and is selected to condense, provided that it is not suppressed by a large tetragonal distortion. We thus focus on T_z and omit the index z .

Following the standard notation for spin-1 condensates, we express complex $T = \mathbf{u} + i\mathbf{v}$ using two real fields \mathbf{u}, \mathbf{v} . The ordered dipolar moment residing on Van Vleck transition $s \leftrightarrow T$ is then $\mathbf{m} = 2\sqrt{6}\mathbf{v}$ [3]. Assuming either FM order (condensation prescribed by $T \rightarrow i\mathbf{v}$) or AF order ($T \rightarrow \pm i\mathbf{v}$ in a Néel pattern), we evaluate the classical energy of the T -condensate and add the energy of the f -bands polarized due to the condensed T . Doing so, we replace s_i by $\sqrt{1-x-v^2}$ to incorporate the constraint on average. The resulting total energy $E(v) = E_T + E_{\text{band}}$ is minimized with respect to the condensate strength v and compared for the individual

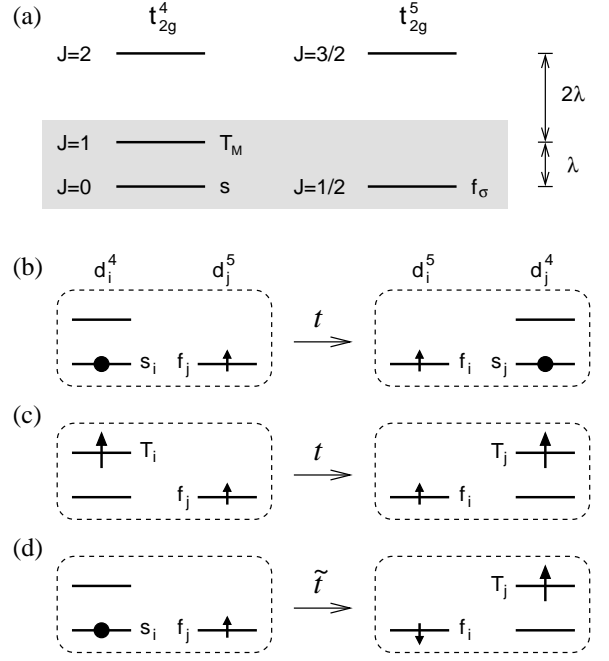


FIG. 1. (a) Spin-orbital level structure of t_{2g}^4 and t_{2g}^5 configurations. Lowest states including singlet s and triplet T_M states of d^4 , and pseudospin 1/2 f_σ states of d^5 configurations form a basis for effective low-energy Hamiltonian. (b)-(d) Schematics of electron hoppings that lead to Eqs. (2) and (3): (b) Free motion of a doped fermion f_σ in a singlet background. (c) Fermion hopping is accompanied by a triplon backflow supporting double-exchange type ferromagnetism. (d) Fermionic hopping generates a singlet-triplet excitation. This process leads to a coupling between Stoner continuum and T -moments promoting magnetic condensation.

phases: FM, AF, and PM ($v = 0$). The condensate energy amounts to $E_T = [\lambda \pm \frac{11}{6}K(1-x-v^2)]v^2$, with the $+/-$ sign for FM/AF phase, respectively. The band energy $E_{\text{band}} = \sum_{\mathbf{k}\sigma} \varepsilon_{\mathbf{k}\sigma} n_{\mathbf{k}\sigma}$ is calculated for a particular doping level $x = \sum_{\mathbf{k}\sigma} n_{\mathbf{k}\sigma}$ using the band dispersion $\varepsilon_{\mathbf{k}\sigma} = -4(t_1 - \sigma t_2)\gamma_{\mathbf{k}}$ where $\gamma_{\mathbf{k}} = \frac{1}{2}(\cos k_x + \cos k_y)$. The hopping parameter t_1 stemming from h_1 reads as $t_1 \simeq t(1-x)$ and $t_1 \simeq t(1-x-2v^2)$ for FM and AF, respectively. This captures the double-exchange nature of h_1 – only FM-aligned T allow for a free motion of f , while AF order of T blocks it. The parameter t_2 quantifies the polarization of the bands by virtue of h_2 and is nonzero in FM case only: $t_2 = \frac{2}{3}\tilde{t}v\sqrt{1-x-v^2}$.

Shown in Fig. 2 are the resulting phase diagrams along with the total ordered moment $m[\mu_B] = 2\sqrt{6}v + n_\uparrow - n_\downarrow$. In both phase diagrams for constant \tilde{t}/λ [Fig. 2(a,b)] at $x = 0$ we recover the QCP of the d^4 model. Nonzero doping causes a suppression of the AF phase via the double-exchange mechanism in h_1 , and an appearance of FM phase strongly supported by h_2 that directly couples the moment $\mathbf{m} \sim \mathbf{v}$ of T exciton to the fermionic spin σ_{ij} , promoting magnetic condensation. With increasing \tilde{t} the FM phase quickly extends as seen also in Fig. 2(c,d)

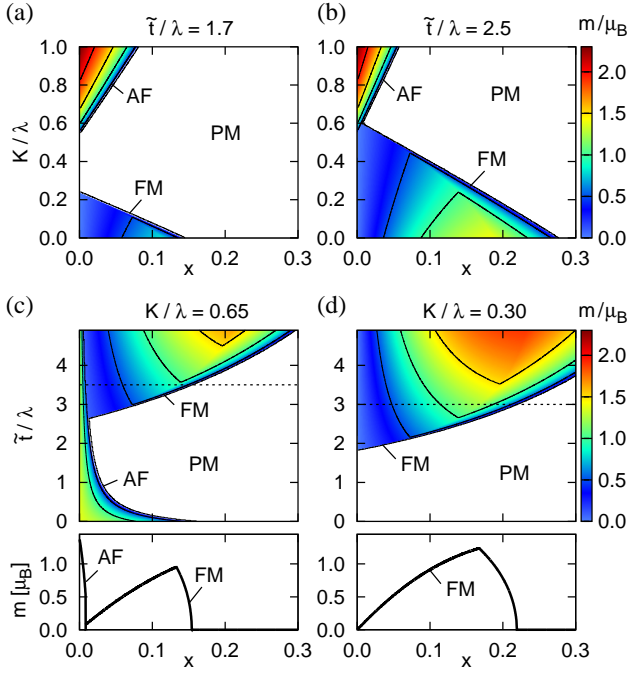


FIG. 2. (Color online) (a,b) Phase diagrams and the ordered magnetic moment value for varying doping x and K/λ keeping fixed \tilde{t}/λ of 1.7 and 2.5. (c) Phase diagram for varying doping and \tilde{t}/λ and fixed $K = 0.65\lambda$ above the critical $K_c = \frac{6}{11}\lambda$ of the d^4 system. Bottom panel shows $m(x)$ along the cut at $\tilde{t}/\lambda = 3.5$. (d) The same for $K = 0.3\lambda$ and the cut at $\tilde{t}/\lambda = 3$.

containing the phase diagrams for constant $K/\lambda = 0.65$ (selected to roughly reproduce experimental value $1.3\mu_B$ for Ca_2RuO_4 [18]) and $K/\lambda = 0.30$. The constant \tilde{t}/λ cut in Fig. 2(c) is strongly reminiscent of the phase diagram of La-doped Ca_2RuO_4 [6, 7, 20], where the AF phase is almost immediately replaced by the FM phase present up to a certain doping level. To estimate realistic values of \tilde{t}/λ , we assume $t_0 \sim 300$ meV. Large SOC in d^4 Ir^{5+} with $\lambda \sim 200$ meV [22–24] leads to $\tilde{t}/\lambda \sim 1$ and places it strictly to the AF/PM (c) or PM/PM (d) regime. In contrast to this, moderate $\lambda \sim 70 - 80$ meV in Ru^{4+} [2, 25] makes the FM phase easily accessible.

Spin susceptibility, emergence of paramagnons.— The tendency toward FM ordering naturally manifests itself in the dynamic spin response of the coupled \mathbf{T} -exciton and f -band system. Here we study it in detail for the PM phase, focusing again on T_z being the closest to condense. The magnetic moment \mathbf{m} is carried mainly by the dipolar component $\mathbf{v} = (\mathbf{T} - \mathbf{T}^\dagger)/2i$ of triplons so that the dominant contribution to the spin susceptibility is given by the \mathbf{v} -susceptibility $\chi(\mathbf{q}, \omega)$. To evaluate it, we replace $s_i \rightarrow \sqrt{1-x-n_{Ti}}$, and decouple h_1 (2) into f and T parts on a mean-field level. This yields a fermionic Hamiltonian $\mathcal{H}_f = \sum_{\mathbf{k}\sigma} \varepsilon_{\mathbf{k}} f_{\mathbf{k}\sigma}^\dagger f_{\mathbf{k}\sigma}$ with $\varepsilon_{\mathbf{k}} = -4t(1-x)\gamma_{\mathbf{k}}$, and a quadratic form for T_z boson: $\mathcal{H}_T = \sum_{\mathbf{q}} [A_{\mathbf{q}} T_{\mathbf{q}}^\dagger T_{\mathbf{q}} - \frac{1}{2} B_{\mathbf{q}} (T_{\mathbf{q}} T_{-\mathbf{q}} + T_{\mathbf{q}}^\dagger T_{-\mathbf{q}}^\dagger)]$.

Here, $A_{\mathbf{q}} = \lambda + 4t\langle n_{ij} \rangle (1 - \gamma_{\mathbf{q}}) + K(1-x)\gamma_{\mathbf{q}}$, $B_{\mathbf{q}} = \frac{5}{6}K(1-x)\gamma_{\mathbf{q}}$, and $\langle n_{ij} \rangle = \sum_{\mathbf{k}\sigma} \gamma_{\mathbf{k}} n_{\mathbf{k}\sigma}$. Bogoliubov diagonalization provides the bare triplon dispersion $\omega_{\mathbf{q}} = (A_{\mathbf{q}}^2 - B_{\mathbf{q}}^2)^{1/2}$ and the bare \mathbf{v} -susceptibility $\chi_0(\mathbf{q}, \omega) = \frac{1}{2}(A_{\mathbf{q}} - B_{\mathbf{q}})/[\omega_{\mathbf{q}}^2 - (\omega + i\delta)^2]$. The susceptibility is further renormalized by the coupling h_2 (3), which can be viewed as an interaction between a dipolar component \mathbf{v} of the triplons and the Stoner continuum of f -fermions:

$$\mathcal{H}_{\text{int}} = g \sum_{\mathbf{q}} v_{\mathbf{q}} \tilde{\sigma}_{-\mathbf{q}}, \quad \tilde{\sigma}_{-\mathbf{q}} = \sum_{\mathbf{k}} \Gamma_{\mathbf{k}\mathbf{q}} f_{\mathbf{k}+\mathbf{q},\alpha}^\dagger \tau_{\alpha\beta}^z f_{\mathbf{k},\beta}. \quad (4)$$

The coupling constant $g = \frac{8}{3}\tilde{t}\sqrt{1-x}$, and the vertex $\Gamma_{\mathbf{k}\mathbf{q}} = \frac{1}{2}(\gamma_{\mathbf{k}} + \gamma_{\mathbf{k}+\mathbf{q}})$ is close to 1 in the limit of small \mathbf{k} , \mathbf{q} . By treating this coupling on a RPA level, we arrive at the full \mathbf{v} -susceptibility $\chi = \chi_0/(1 - \chi_0\Pi)$ with the \mathbf{v} -selfenergy

$$\Pi(\mathbf{q}, \omega) = g^2 \sum_{\mathbf{k}\sigma} \Gamma_{\mathbf{k}\mathbf{q}}^2 \frac{n_{\mathbf{k}\sigma} - n_{\mathbf{k}+\mathbf{q}\sigma}}{\varepsilon_{\mathbf{k}+\mathbf{q}} - \varepsilon_{\mathbf{k}} - \omega - i\delta}. \quad (5)$$

The interplay of the coupled excitonic and band spin responses is demonstrated in Fig. 3. The high-energy component of χ linked to χ_0 follows the bare triplon dispersion $\omega_{\mathbf{q}}$. In an undoped system, due to the AF K -interaction, $\omega_{\mathbf{q}}$ has a minimum at $\mathbf{q} = (\pi, \pi)$ and χ_0 would be most intense there. By doping, the double exchange mechanism in h_1 disfavoring AF correlations pushes $\omega_{\mathbf{q}}$ up near (π, π) . Further, due to a dynamical mixing (3,4) of triplons with the fermionic continuum, the low-energy component of χ gains spectral weight as \tilde{t}/λ approaches the critical value, and a gradually softening FM-paramagnon is formed [see Fig. 3(b)]. The emergence of the paramagnon and the increase of its spectral weight is shown in detail in Fig. 3(e). Finally, once the critical \tilde{t}/λ is reached, triplons, whose spectral weight was pulled down by the coupling to the Stoner continuum, condense and the FM order sets in, signaled by the divergence of $\chi(\mathbf{q} = 0, \omega = 0)$ [cf. 3(c,d)].

Triplet pairing.— Intense paramagnons emerging in the proximity to the FM phase may serve as mediators of a triplet pairing interaction [26]. In the following, we perform semiquantitative estimates for this triplet SC.

While the dominant contribution to the pairing strength is due to the v_z -fluctuations, in order to assess the structure of the triplet order parameter, the full coupling $\mathcal{H}_{\text{int}} = g \sum_{\mathbf{q}} \mathbf{v}_{\mathbf{q}} \cdot \tilde{\boldsymbol{\sigma}}_{-\mathbf{q}}$ leading to the effective interaction $-\frac{1}{2}g^2 \sum_{\mathbf{q}\alpha} \chi_{\alpha}(\mathbf{q}, \omega = 0) \tilde{\sigma}_{\mathbf{q}}^{\alpha} \tilde{\sigma}_{-\mathbf{q}}^{\alpha}$ has to be considered. The v_{α} -susceptibility χ_{α} for $\alpha = x, y$ may be calculated the same way as χ_z above, using now $A_{\mathbf{q}}^{\alpha} = A_{\mathbf{q}}^z + [\frac{6}{5}t\langle n_{ij} \rangle - \frac{1}{6}K(1-x)] \cos q_{\alpha}$ and $B_{\mathbf{q}}^{\alpha} = B_{\mathbf{q}}^z - \frac{1}{12}K(1-x) \cos q_{\alpha}$. The coupling vertex for v_x and v_y obtains an additional contribution, $\Gamma_{\mathbf{k}\mathbf{q}}^{\alpha} = \Gamma_{\mathbf{k}\mathbf{q}}^z - \frac{3}{4}[\cos k_{\alpha} + \cos(k_{\alpha} + q_{\alpha})]$. The resulting BCS interaction in terms of $t_{+1\mathbf{k}} = f_{\mathbf{k}\uparrow} f_{-\mathbf{k}\uparrow}$, $t_{0\mathbf{k}} = \frac{1}{\sqrt{2}}(f_{\mathbf{k}\downarrow} f_{-\mathbf{k}\uparrow} + f_{\mathbf{k}\uparrow} f_{-\mathbf{k}\downarrow})$,

and $t_{-1\mathbf{k}} = f_{\mathbf{k}\downarrow}f_{-\mathbf{k}\downarrow}$ takes the form

$$\mathcal{H}_{\text{BCS}} = -\frac{1}{2} \sum_{\mathbf{k}\mathbf{k}'} \left[V_z (t_1^\dagger t_1 + t_{-1}^\dagger t_{-1})_{\mathbf{k}\mathbf{k}'} + (V_x - V_y)(t_1^\dagger t_{-1} + t_{-1}^\dagger t_1)_{\mathbf{k}\mathbf{k}'} + (V_x + V_y - V_z)t_{0\mathbf{k}}^\dagger t_{0\mathbf{k}'} \right], \quad (6)$$

where V_α denotes the properly symmetrized $V_{\alpha\mathbf{k}\mathbf{k}'} = g^2(\Gamma_{\mathbf{k},\mathbf{k}'-\mathbf{k}}^\alpha)^2 \frac{1}{2}[\chi_\alpha(\mathbf{k}-\mathbf{k}') - \chi_\alpha(\mathbf{k}+\mathbf{k}')]$. Decomposed into the Fermi surface harmonics, the BCS interaction is well approximated by $V_{z\mathbf{k}\mathbf{k}'} \approx 2V_0 \cos(\phi_{\mathbf{k}} - \phi_{\mathbf{k}'})$ and $(V_x - V_y)_{\mathbf{k}\mathbf{k}'} \approx 2V_1 \cos(\phi_{\mathbf{k}} + \phi_{\mathbf{k}'})$ with $V_{0,1} > 0$ [see Fig. 3(d) and Fig. 4(a)]. The relatively small $V_1 \ll V_0$ fixes the relative phase of the t_{+1} and t_{-1} pairs so that the SC order parameter becomes $\Delta_{\pm 1\mathbf{k}} = \Delta e^{\pm i\phi_{\mathbf{k}}}$. This ordering type is captured by the \mathbf{d} -vector $\mathbf{d} = -i\Delta(\sin \phi_{\mathbf{k}}, \cos \phi_{\mathbf{k}}, 0) \sim \hat{x}k_y + \hat{y}k_x$ shown in Fig. 4(b). In the classification of Ref. 28, it forms the Γ_4^- irreducible representation of tetragonal group D_{4h} . However, this

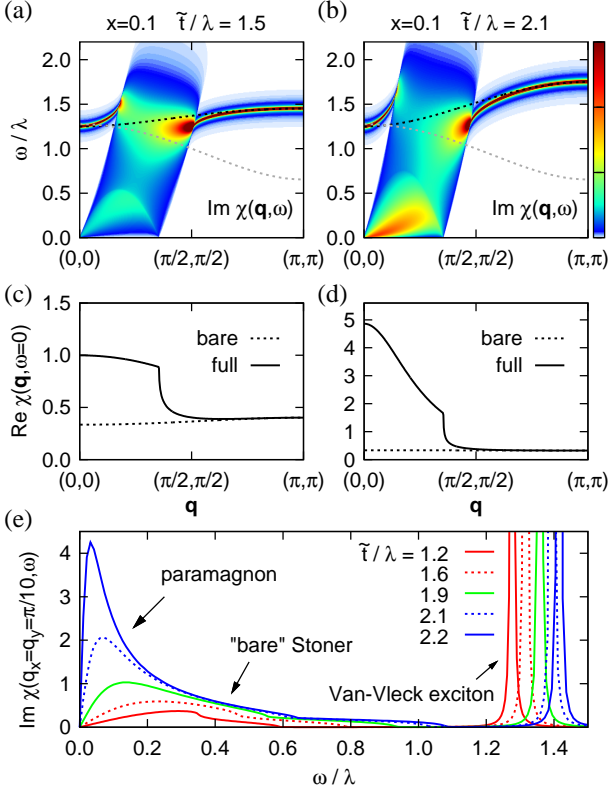


FIG. 3. (Color online) (a) Imaginary part of the v_z -susceptibility $\chi(\mathbf{q}, \omega)$ in (π, π) -direction calculated for $x = 0.1$, $\tilde{t}/\lambda = 1.5$, $K/\lambda = 0.3$. $\chi(\mathbf{q}, \omega)$ is shown in units of λ^{-1} . Black (gray) dashed line shows the bare triplon dispersion for $x = 0.1$ ($x = 0$). (b) The same for $\tilde{t}/\lambda = 2.1$ closer to the FM transition point $\tilde{t}/\lambda \approx 2.25$. (c,d) The static susceptibility that corresponding to panels (a) and (b). (e) Imaginary part of $\chi(\mathbf{q}, \omega)$ at $\mathbf{q} = (\pi/10, \pi/10)$ for several values of \tilde{t}/λ gradually approaching the FM transition point.

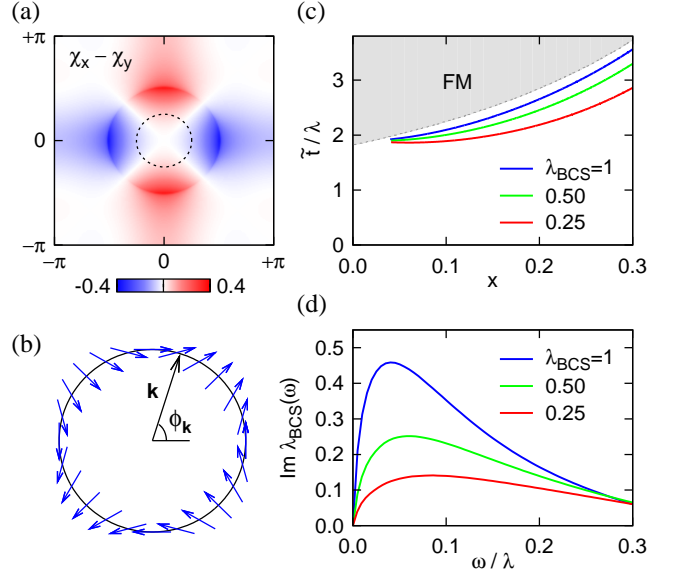


FIG. 4. (Color online) (a) Combination $(\chi_x - \chi_y)_{\omega=0}$ that determines the symmetry of the pairing potential $V_x - V_y$. The parameters are the same as in Fig. 3(b,d). Dashed circle indicates the Fermi surface. (b) Representation of $\Delta_{\pm 1\mathbf{k}} = \Delta e^{\pm i\phi_{\mathbf{k}}}$ using the \mathbf{d} -vector along the Fermi surface. (c) Contours of $\lambda_{\text{BCS}} = V_0 N$ in the phase diagram of Fig. 2(d). (d) Imaginary part of ω -dependent $\lambda_{\text{BCS}}(\omega)$ for $x = 0.1$ and the values of \tilde{t}/λ corresponding to $\lambda_{\text{BCS}} = 1, 0.5$, and 0.25 .

result applies to cubic symmetry case. Lattice distortions that cause splitting among $T_{x,y,z}$ and modify the pseudospin wave functions may in fact offer a possibility to “tune” the symmetry of the order parameter. If distortions favor $T_{x,y}$, the potentials $V_{x,y}$ are expected to dominate in Eq. 6, supporting the chiral t_0 -pairing represented by the last term in (6).

Data in Fig. 4(c,d) serve as a basis for a rough T_c estimate. Fig. 4(c) shows the BCS parameter $\lambda_{\text{BCS}} \approx V_0 N$ (N is DOS per spin component of the f -band) which attains sizable values near the FM phase boundary, where the paramagnons are intense. To avoid complex physics near the very vicinity of the FM QCP [29–31], we take a conservative upper limit $\lambda_{\text{BCS}} \approx 0.5$. Extending V_0 by the ω -dependence of the underlying $\chi_z(\mathbf{q}, \omega)$, we define $\lambda_{\text{BCS}}(\omega)$. Its imaginary part to be understood as the conventional $\alpha^2 F$ is plotted in Fig. 4(d) yielding an estimate of the BCS cutoff $\Omega \lesssim 0.1\lambda$. With $\lambda \sim 100$ meV, this gives $T_c \approx \Omega e^{-1/\lambda_{\text{BCS}}}$ of about 10 K.

In conclusion, we have explored the doping effects in spin-orbit d^4 Mott insulators. The results show that the doped electrons moving in the d^4 background firmly favor ferromagnetism, explaining *e.g.* the observed behavior of La-doped Ca_2RuO_4 . In the paramagnetic phase near the FM QCP, the incipient FM correlations are manifested by intense paramagnons that may provide a triplet pairing.

We thank G. Jackeli for useful comments. J.C. acknowledges support by the Czech Science Foundation

(GAČR) under Project No. 15-14523Y and ERDF under Project CEITEC (CZ.1.05/1.1.00/02.0068).

-
- [1] M. Imada, A. Fujimori, and Y. Tokura, *Rev. Mod. Phys.* **70**, 1039 (1998).
 - [2] A. Abragam and B. Bleaney, *Electron Paramagnetic Resonance of Transition Ions* (Clarendon, Oxford, 1970).
 - [3] G. Khaliullin, *Phys. Rev. Lett.* **111**, 197201 (2013).
 - [4] O.N. Meetei, W.S. Cole, M. Randeria, and N. Trivedi, *Phys. Rev. B* **91**, 054412 (2015).
 - [5] A. Jain, M. Krautloher, J. Porras, G.H. Ryu, D.P. Chen, D.L. Abernathy, J.T. Park, A. Ivanov, J. Chaloupka, G. Khaliullin, B. Keimer, and B.J. Kim, arXiv:1510.07011.
 - [6] G. Cao, S. McCall, V. Dobrosavljevic, C.S. Alexander, J.E. Crow, and R.P. Guertin, *Phys. Rev. B* **61**, R5053 (2000).
 - [7] G. Cao, C.S. Alexander, S. McCall, J.E. Crow, and R.P. Guertin, *J. Magn. Magn. Mater.* **226-230**, 235 (2001).
 - [8] F. Nakamura, M. Sakaki, Y. Yamanaka, S. Tamaru, T. Suzuki, and Y. Maeno, *Sci. Rep.* **3**, 2536 (2013).
 - [9] C.R. Hughes, T. Harada, R. Ashoori, A.V. Boris, H. Hilgenkamp, M.E. Holtz, L. Li, J. Mannhart, D.A. Muller, D.G. Schlom, A. Soukiassian, X. Renshaw Wang, and H. Boschker (unpublished).
 - [10] S. Nakatsuji, S. Ikeda, and Y. Maeno, *J. Phys. Soc. Jpn.* **66**, 1868 (1997).
 - [11] Y. Miura, Y. Yasui, M. Sato, N. Igawa, and K. Kakurai, *J. Phys. Soc. Jpn.* **76**, 033705 (2007).
 - [12] M. Bremholm, S.E. Dutton, P.W. Stephens, and R.J. Cava, *J. Solid State Chem.* **184**, 601 (2011).
 - [13] G. Cao, T.F. Qi, L. Li, J. Terzic, S.J. Yuan, L.E. DeLong, G. Murthy, and R.K. Kaul, *Phys. Rev. Lett.* **112**, 056402 (2014).
 - [14] Y. Shi, Y. Guo, Y. Shirako, W. Yi, X. Wang, A.A. Belik, Y. Matsushita, H.L. Feng, Y. Tsujimoto, M. Arai, N. Wang, M. Akaogi, and K. Yamaura, *J. Am. Chem. Soc.* **135**, 16507 (2013).
 - [15] P. Khalifah, R. Osborn, Q. Huang, H.W. Zandbergen, R. Jin, Y. Liu, D. Mandrus, and R.J. Cava, *Science* **297**, 2237 (2002).
 - [16] S. Lee, J.-G. Park, D.T. Adroja, D. Khomskii, S. Streltsov, K.A. McEwen, H. Sakai, K. Yoshimura, V.I. Anisimov, D. Mori, R. Kanno, and R. Ibberson, *Nat. Mater.* **5**, 471 (2006).
 - [17] Hua Wu, Z. Hu, T. Burnus, J.D. Denlinger, P.G. Khalifah, D.G. Mandrus, L.-Y. Jang, H.H. Hsieh, A. Tanaka, K.S. Liang, J.W. Allen, R.J. Cava, D.I. Khomskii, and L.H. Tjeng, *Phys. Rev. Lett.* **96**, 256402 (2006).
 - [18] M. Braden, G. André, S. Nakatsuji, and Y. Maeno, *Phys. Rev. B* **58**, 847 (1998).
 - [19] A. Akbari and G. Khaliullin, *Phys. Rev. B* **90**, 035137 (2014).
 - [20] For a detailed comparison, one has to keep in mind polaronic and phase coexistence effects [21] generic to weakly doped Mott insulators, and deviations from two dimensionality.
 - [21] W. Brzezicki, A.M. Oleś, and M. Cuoco, *Phys. Rev. X* **5**, 011037 (2015).
 - [22] B.N. Figgis and M.A. Hitchman, *Ligand Field Theory and Its Applications* (Wiley-VCH, New York, 2000).
 - [23] J. Kim, D. Casa, M.H. Upton, T. Gog, Y.-J. Kim, J.F. Mitchell, M. van Veenendaal, M. Daghofer, J. van den Brink, G. Khaliullin, and B.J. Kim, *Phys. Rev. Lett.* **108**, 177003 (2012).
 - [24] Note a relation $\lambda = \xi/2S$ between spin-orbit coupling constant λ for spin $S = 1$ and the single-electron one ξ [2].
 - [25] T. Mizokawa, L.H. Tjeng, G.A. Sawatzky, G. Ghiringhelli, O. Tjernberg, N.B. Brookes, H. Fukazawa, S. Nakatsuji, and Y. Maeno, *Phys. Rev. Lett.* **87**, 077202 (2001).
 - [26] We recall that the pseudospins are spin-orbit entangled objects [27], and hence a pseudospin triplet is in fact a mixture of real-spin singlets and triplets.
 - [27] G. Khaliullin, *Prog. Theor. Phys. Suppl.* **160**, 155 (2005).
 - [28] M. Sigrist and K. Ueda, *Rev. Mod. Phys.* **63**, 239 (1991).
 - [29] A.V. Chubukov, A.M. Finkelstein, R. Haslinger, and D.K. Morr, *Phys. Rev. Lett.* **90**, 077002 (2003).
 - [30] A.V. Chubukov, C. Pépin, and J. Rech, *Phys. Rev. Lett.* **92**, 147003 (2004).
 - [31] A.V. Chubukov and D.L. Maslov, *Phys. Rev. Lett.* **103**, 216401 (2009).